

## Rab-GAP TBC1D4 (AS160) is dispensable for the renal control of sodium and water homeostasis but regulates GLUT4 in mouse kidney

Marianna Di Chiara,<sup>1,2</sup> Bob Glaudemans,<sup>3</sup> Dominique Loffing-Cueni,<sup>1</sup> Alex Odermatt,<sup>4,5</sup> Hadi Al-Hasani,<sup>6</sup> Olivier Devuyst,<sup>2,3,5</sup> Nouridine Faresse,<sup>1,2,5</sup> and Johannes Loffing<sup>1,2,5</sup>

<sup>1</sup>Institute of Anatomy, University of Zurich, Zurich, Switzerland; <sup>2</sup>Zurich Center of Integrative Human Physiology, University of Zurich, Zurich, Switzerland; <sup>3</sup>Institute of Physiology, University of Zurich, Zurich, Switzerland; <sup>4</sup>Division of Molecular and Systems Toxicology, Pharmazentrum, University of Basel, Basel, Switzerland; <sup>5</sup>National Center of Competence in Research “Kidney.CH,” Switzerland; and <sup>6</sup>German Diabetes Center, Leibniz Center for Diabetes Research, Heinrich-Heine-University and German Center for Diabetes Research, Düsseldorf, Germany

Submitted 31 March 2015; accepted in final form 29 August 2015

**Di Chiara M, Glaudemans B, Loffing-Cueni D, Odermatt A, Al-Hasani H, Devuyst O, Faresse N, Loffing J.** Rab-GAP TBC1D4 (AS160) is dispensable for the renal control of sodium and water homeostasis but regulates GLUT4 in mouse kidney. *Am J Physiol Renal Physiol* 309: F779–F790, 2015. First published September 2, 2015; doi:10.1152/ajprenal.00139.2015.—The Rab GTPase-activating protein TBC1D4 (AS160) controls trafficking of the glucose transporter GLUT4 in adipocytes and skeletal muscle cells. TBC1D4 is also highly abundant in the renal distal tubule, although its role in this tubule is so far unknown. In vitro studies suggest that it is involved in the regulation of renal transporters and channels such as the epithelial sodium channel (ENaC), aquaporin-2 (AQP2), and the Na<sup>+</sup>-K<sup>+</sup>-ATPase. To assess the physiological role of TBC1D4 in the kidney, wild-type (TBC1D4<sup>+/+</sup>) and TBC1D4-deficient (TBC1D4<sup>-/-</sup>) mice were studied. Unexpectedly, neither under standard nor under challenging conditions (low Na<sup>+</sup>/high K<sup>+</sup>, water restriction) did TBC1D4<sup>-/-</sup> mice show any difference in urinary Na<sup>+</sup> and K<sup>+</sup> excretion, urine osmolality, plasma ion and aldosterone levels, and blood pressure compared with TBC1D4<sup>+/+</sup> mice. Also, immunoblotting did not reveal any change in the abundance of major renal sodium- and water-transporting proteins [Na-K-2Cl cotransporter (NKCC2), NaCl cotransporter (NCC), ENaC, AQP2, and the Na<sup>+</sup>-K<sup>+</sup>-ATPase]. However, the abundance of GLUT4, which colocalizes with TBC1D4 along the distal nephron of TBC1D4<sup>+/+</sup> mice, was lower in whole kidney lysates of TBC1D4<sup>-/-</sup> mice than in TBC1D4<sup>+/+</sup> mice. Likewise, primary thick ascending limb (TAL) cells isolated from TBC1D4<sup>-/-</sup> mice showed an increased basal glucose uptake and an abrogated insulin response compared with TAL cells from TBC1D4<sup>+/+</sup> mice. Thus, TBC1D4 is dispensable for the regulation of renal Na<sup>+</sup> and water transport, but may play a role for GLUT4-mediated basolateral glucose uptake in distal tubules. The latter may contribute to the known anaerobic glycolytic capacity of distal tubules during renal ischemia.

hypertension; ion transport; distal tubule; glucose

ARTERIAL BLOOD PRESSURE CONTROL critically depends on the regulation of renal sodium (Na<sup>+</sup>) and water excretion. The fine tuning of renal Na<sup>+</sup> and water excretion occurs in the renal distal tubules that are localized downstream of the macula densa and comprise the distal convoluted tubule (DCT), the connecting tubule (CNT), and the collecting duct (CD) (36, 44). In the DCT, the apical Na<sup>+</sup> transport is mediated by the thiazide-sensitive NaCl cotransporter (NCC), whereas in the CNT and CD transport is mediated by the amiloride-sensitive

epithelial Na<sup>+</sup> channel (ENaC). In several species, including mice and humans, NCC and ENaC are coexpressed in the short end portion of the DCT, called DCT2 (44). The basolateral Na<sup>+</sup> transport is mediated by the ubiquitously expressed Na<sup>+</sup>-K<sup>+</sup>-ATPase. The renal water reabsorption depends on the abundance of aquaporin-2 (AQP2) water channels in the luminal membrane of the CNT and CD. The activity of NCC, ENaC, Na<sup>+</sup>-K<sup>+</sup>-ATPase, and AQP2 is regulated (at least in part) by an aldosterone- and/or vasopressin-induced insertion of these proteins into the plasma membrane, suggesting that the control of intracellular trafficking of these proteins is a critical mechanism for the renal maintenance of salt and water homeostasis and hence blood pressure (36, 39).

The intracellular trafficking of protein-bearing membrane vesicles is controlled by the activity of Rab proteins, which belong to the family of small GTPases (53). So far more than 50 mammalian Rab proteins have been identified. Each of these may regulate a specific step in the intracellular transport of membrane vesicles, including their budding from a donor compartment, their transport along the cytoskeleton, and their fusion with an acceptor compartment (58). Rab proteins in turn are controlled by RabGTPase-activating proteins (Rab-GAP), which change the conformation of Rab proteins from a GTP-bound (active) to a GDP-bound (inactive) state through hydrolysis (7, 53). One of these Rab-GAP proteins is TBC1D4, which belongs to the family of TBC (Tre-2/Bub2/Cdc16) domain-containing proteins (21). Previous work has identified TBC1D4 as an Akt kinase substrate of 160 kDa (AS160) that regulates the insulin-dependent trafficking of the glucose transporter GLUT4 in adipose tissue and skeletal muscle (28). In its nonphosphorylated state, TBC1D4 (AS160) inhibits GLUT4 trafficking and hence prevents glucose uptake. Upon stimulation with insulin, protein kinase B (PKB)/Akt phosphorylates TBC1D4, which in turn induces its sequestration by 14-3-3 proteins and further activates Rab proteins. Consequently, this favors Rab-mediated transport of GLUT4 storage vesicles to the cell surface, which finally promotes glucose uptake into the cells (28, 50).

In addition to adipose and skeletal muscle tissue, TBC1D4 is also present in the pancreas, lung, heart, brain, and kidney (8, 16, 31, 35, 57). Based on in vitro observations, it was suggested that TBC1D4 modulates the activity and trafficking of transporters and channels involved in sodium and water handling. In MDCK and COS cells, Alves et al. demonstrated that endogenous TBC1D4 interacts with the Na<sup>+</sup>-K<sup>+</sup>-ATPase  $\alpha$ -subunit and that overexpression of TBC1D4 induces an

Address for reprint requests and other correspondence: J. Loffing, Univ. of Zurich, Institute of Anatomy, Winterthurerstrasse 190, 8057 Zurich, Switzerland (e-mail: johannes.loffing@anatom.uzh.ch).

intracellular retention of the  $\text{Na}^+\text{-K}^+\text{-ATPase}$  (3). Liang et al. showed that, in renal epithelial cells of the cortical collecting duct, aldosterone promotes serum-glucocorticoid-regulated kinase 1 (SGK1)-mediated phosphorylation of TBC1D4 and thus regulates the trafficking and insertion of ENaC into the cell membrane (34). Likewise, TBC1D4 knockdown with small-interfering RNA increases AQP2 expression in the plasma membrane of collecting duct-derived mpkCCD cells (27, 29). However, all of these studies were performed in heterologous expression systems or cell lines in vitro. The role of TBC1D4 in the kidney in vivo still remains unclear.

In this study, we used TBC1D4 knockout mice to elucidate the role of TBC1D4 in renal control of sodium and water homeostasis. Our data suggest that TBC1D4 is dispensable for the control of renal  $\text{Na}^+$  and water handling under standard conditions and under conditions that stimulate endogenous aldosterone and vasopressin production. However, we provide in vivo and ex vivo experimental evidence that TBC1D4 does control the GLUT4-dependent glucose uptake in renal distal tubule cells, which may contribute to their known glycolytic capacity.

## MATERIALS AND METHODS

**Animals.** All animal studies were conducted according to the Swiss animal welfare regulations and after approval by the veterinarian office of the Canton of Zurich, Switzerland. For the experiments, age-matched wild-type (TBC1D4<sup>+/+</sup>) and TBC1D4-deficient (TBC1D4<sup>-/-</sup>) (13, 35) mice were used. For the physiological data collection, mice were kept in single mouse metabolic cages (Techniplast, Buguggiate, Italy) for 4 days. Data (body weight, food and water intake, urine excretion) were evaluated every 24 h. Mice were fed a standard diet (SD) (Ssniff Spezialdiäten, Soest, Germany) with 0.19%  $\text{Na}^+$  mixed with double-distilled  $\text{H}_2\text{O}$  1:1. For low  $\text{Na}^+$ /high  $\text{K}^+$  diet (LNa/HKD), 7.7% of KCl was added to a low  $\text{Na}^+$ -diet (<0.03%  $\text{Na}^+$  and 0.97%  $\text{K}^+$ ) to reach a  $\text{K}^+$  content of 5%. Mice were kept for 10 days on LNa/HKD before experimental analysis. Mice had free access to tap water. Only for the water restriction experiment, the water bottle was removed and mice were given access to water only via food, which was added to the dried powder diet in a 1:1 ratio. Mice were kept for 24 h on this regime before experimental analysis.

**Blood pressure measurements.** Systolic blood pressure (SBP) was determined in conscious mice using the non-invasive tail cuff method (BP2000; Visitech Systems, Apex, NC) (54) and the provided software for data analysis. Mice were adapted for 3 days before the experiments. Measurements were carried out daily between 10:00 A.M. and 12:00 P.M. SBP was calculated in millimeters mercury out of an average of 20 possible corrected single measurements per day and mouse for three consecutive days.

**Biochemical measurements.** Urinary aldosterone levels were measured using the aldosterone EIA kit (Cayman Chemicals, Ann Arbor, MI). Values were normalized to urine volumes and expressed in nanograms per 24 h. Urinary ion concentrations ( $\text{Na}^+$ ,  $\text{K}^+$ ,  $\text{Mg}^{2+}$ ) were determined using an automated 850 professional IC ion chromatograph (Metrohm, Herisau, Switzerland) and/or by flame photometry (EFOX 5053; Eppendorf, Hamburg, Germany). Creatinine levels were measured as described (52). Urinary osmolarity was measured with a digital osmometer (Roebeling, Berlin, Germany). Due to evaporation of urine during the sampling period, measured urine parameters are higher than expected to be in vivo. At the end of the experiments, mice were anesthetized with 4% isoflurane (CliniPharm, Zurich, Switzerland). Blood glucose was measured from a drop of the tail tip with the Accu-Chek Aviva System (Roche, Basel, Switzerland). Blood (300  $\mu\text{l}$ ) was drawn from the right atrium or the

abdominal vein; 100  $\mu\text{l}$  of blood were immediately measured in a blood gas analyzer (ABL800 Flex; Radiometer, Copenhagen, Denmark) through capillary tubes; and 200  $\mu\text{l}$  blood were centrifuged at 800 g for 3 min at 4°C to harvest the plasma. Plasma insulin levels were determined using the mouse insulin ELISA kit and the ultrasensitive mouse insulin ELISA kit (ALPCO Diagnostics, Salem, NH). Plasma aldosterone and corticosterone levels were measured by mass spectrometry as described (52). For harvesting of kidneys, mice were perfused through the heart with  $1\times$  PBS. Kidneys were immediately frozen in liquid nitrogen and stored at  $-80^\circ\text{C}$ .

**Generation of TBC1D1 antibody.** An anti-TBC1D1 antibody was generated by immunizing rabbits with a synthetic peptide corresponding to an  $\text{NH}_2$ -terminal amino acid sequence of mouse TBC1D1 (EAITFTARKHPFPNEVSVDFC). The COOH-terminal cysteine (C) residue was added to allow coupling of the peptide to keyhole limpet hemocyanin. Antisera were affinity purified against the immunizing peptide and used for immunoblotting as described below. Peptide synthesis, immunization of rabbits, and antibody purification were custom made (Pineda Ab-Service, Berlin, Germany).

**Preparation of tissues, subcellular preparation, and immunoblotting.** Whole kidney homogenization was performed as described (52). For preparation of cytosolic- and membrane-enriched protein fractions, 400  $\mu\text{l}$  of the kidney homogenate were centrifuged at 100,000 g for 1 h at 4°C. The supernatant (cytosolic fraction) was transferred to a new tube, and the pellet (membrane fraction) was sonicated (Bandelin Sonoplus) for 15 s at 15% power in 300  $\mu\text{l}$  lysis buffer. Protein concentrations were assayed with a Bradford assay (Uptima, Montluçon Cedex, France). Lysates were separated by SDS-PAGE and transferred to nitrocellulose membranes (Whatman Protran; GE Healthcare, Chalfont, UK). Membranes were blocked in blocking buffer (LI-COR Biosciences, Bad Homburg, Germany) (room temperature, 30 min) and incubated with primary antibodies overnight at 4°C. All primary antibodies used are listed in Table 1. Noncommercially available antibodies were characterized in the referenced studies. For visualization, blots were incubated with a dye-conjugated secondary IgG (room temperature, 2 h). The Odyssey infrared-scanner detection system from LI-COR was used. Densitometric analyses were performed with the supplied software.

**Quantitative real-time PCR.** For total RNA extraction, kidneys were homogenized using the rotor-stator Polytron PT 2100 homogenizer (Kinematica, Lucerne, Switzerland) in RNA lysis buffer of the SV total RNA isolation system kit (Promega, Madison, WI). RNA extraction protocol was continued following the manufacturer's instructions. Relative mRNA expression levels were determined through quantitative real-time PCR with the LightCycler 480 II (Roche). Data were analyzed using the LightCycler 480 Instrument Software version 1.5. The following primers were used: TBC1D4 (NM\_001081278) 5'-GCGCCAACGAATCTCTGGTGGAT-3' and 5'-GCATGGGGCAGGTCTCGCAC-3', GLUT4 (NM\_009204) 5'-ACACTGGTCCTAGCTGTATTCT-3' and 5'-CCAGCCACGTTGCATTGTA-3', and insulin receptor (IR) (NM\_010568.2) 5'-TCACGGAGTATGTCCCCAGTAGGC-3' and 5'-ATACCAGGGCACCTCTCCAGG-3', forward and reverse primer, respectively.

**Microarray analyses on complex object parametric analysis and sorting DCTs.** TBC1D4<sup>+/+</sup> and TBC1D4<sup>-/-</sup> mice (35) were crossed with transgenic (tg) PV-EGFP<sup>w/tg</sup> mice expressing enhanced green fluorescent protein (EGFP) under control of the parvalbumin promoter (38). Male, 8-wk-old TBC1D4<sup>+/+</sup>  $\times$  PV-EGFP<sup>w/tg</sup> and TBC1D4<sup>-/-</sup>  $\times$  PV-EGFP<sup>w/tg</sup> (4 mice/genotype) were then used to isolate EGFP-positive DCTs in large scale by complex object parametric analysis and sorting (COPAS) as described (41). For transcriptomic analysis, RNA was isolated from isolated DCTs by using the high-pure RNA isolation kit (Roche). RNA quality was assessed with the 2100 Bioanalyzer (Agilent, Santa Clara, CA) and NanoDrop ND-1000 (NanoDrop Technologies, Wilmington, DE), and labeled cDNA from 100 ng RNA was generated by the Functional Genomics

Table 1. Primary antibodies used for IB and IHC

Antibody	Host	Dilution		Source	Reference
		IB	IHC		
TBC1D4	Rabbit	4,000	1,000	Loffing	35
TBC1D1	Rabbit	1,000		This study	This study
GLUT4	Rabbit	10,000	1,000–5,000	Millipore	Catalog-No. 07-1404
GLUT4	Rabbit	10,000	2,000–10,000	Sigma	Catalog-No. G4173
Akt	Rabbit	1,000		Cell Signaling	Catalog-No. 9272
pAkt	Rabbit	1,000		Cell Signaling	Catalog-No. sc7976
ERK1/2	Rabbit	500		SCBT	Catalog-No. sc7976
pERK1/2	Rabbit	500		SCBT	Catalog-No. sc101760
Na <sup>+</sup> -K <sup>+</sup> -ATPase	Rabbit	10,000		Feraille	21
NKCC2	Rabbit	1,000	10,000	Loffing	56
tNCC	Rabbit	10,000		Loffing	52
pT53 NCC	Rabbit	5,000		Loffing	52
pT58 NCC	Rabbit	5,000		Loffing	52
pS71 NCC	Rabbit	5,000		Loffing	52
α-ENaC	Rabbit	1,000		Loffing	52
β-ENaC	Rabbit	7,500		Loffing	56
γ-ENaC	Rabbit	7,500	20,000	Loffing	56
AQP2	Rabbit	5,000	20,000	Loffing	56
β-actin	Mouse	10,000		Sigma	Catalog-No. A1978

IB, immunoblotting; IHC, immunohistochemistry; p, phosphorylated; t, total; AQP2, aquaporin-2.

Center Zurich (FGCZ). Microarray experiments comparing samples of TBC1D4<sup>+/+</sup> × PV-EGFP<sup>wt/tg</sup> and TBC1D4<sup>-/-</sup> × PV-EGFP<sup>wt/tg</sup> mice were performed on Affymetrix 1.1 Mouse Gene Array (Santa Clara, CA), and gene levels were analyzed with the b-fabric system of the FGCZ. The microarray data will be deposited in the Gene Expression Omnibus database (accession no.: GSE67701) of the National Institutes of Health (www.nih.gov).

**Fixation, tissue processing, and immunohistochemistry.** Paraformaldehyde (3%) dissolved in a 0.1 M cacodylate buffer was used to fix mouse kidneys through the abdominal aorta as described previously (37). For immunohistochemistry, all primary antibodies (Table 1) were incubated overnight at 4°C on 4- to 5-μm cryosections. Immunofluorescent pictures were taken with the Leica DM6000B microscope and the LSM510Meta (CarlZeiss, Oberkochen, Germany) confocal microscope. Pictures were processed using the Leica Application Suite Advanced Fluorescence Lite (LAS AF Lite) 2.6.0 software from Leica Microsystems.

**Primary thick ascending limb cell isolation and culture.** Primary thick ascending limb (TAL) cells were prepared from microdissected tubules of 3- to 6-wk-old male mice as described (22). In short, ~50 TAL segments were placed on 0.33-cm<sup>2</sup> collagen-coated PTFE filter membranes (Transwell-COL, pore size 0.4 μm; Corning, Tewksbury, MA) in culture medium (DMEM-F-12; GIBCO-BRL, Breda, The Netherlands) supplemented with 15 mM HEPES (GIBCO-BRL), 0.55 mM sodium pyruvate (GIBCO-BRL), 0.01% nonessential amino acids (GIBCO-BRL), 2% FBS, and a batch of SingleQuots (Lonza BioWhittaker, Verviers, Belgium), pH 7.4, and incubated in a humidified chamber at 37°C and 5% CO<sub>2</sub>. A monolayer of TAL cells developed from the tubular fragments after 12–15 days. Subsequently, the cells were cultured for 2 days in the absence of FBS to allow full differentiation.

**2-[<sup>3</sup>H]deoxyglucose uptake in mouse primary TAL cultures.** GLUT4-specific glucose transport activity was assessed in primary TAL cultures ( $n = 5$ –8) obtained from TBC1D4<sup>+/+</sup> and TBC1D4<sup>-/-</sup> mice ( $n \geq 3$ , each) in the presence or absence of insulin. The uptake protocol was adapted from glucose uptake experiments in fat and muscle cells (14, 31). The day before the experiment, the cultures were incubated overnight in serum- and insulin-free medium. The following day, each culture was washed three times using uptake buffer (150 mM NaCl, 10 mM HEPES, CaCl<sub>2</sub>, 5 mM KCl, and 1 mM MgCl<sub>2</sub>). Next, the TAL cultures were incubated for 30 min in uptake buffer supplemented with 100 μM D-glucose with or without 300 nM

insulin. The transport of glucose was determined by 2-[<sup>3</sup>H]deoxyglucose (Perkin-Elmer, Waltham, MA) uptake experiments (uptake buffer supplemented with 0.5 μCi/ml 2-[<sup>3</sup>H]deoxyglucose and 100 μM D-glucose). After 15 min, the uptake was stopped by adding 50 μM cytochalasin B (Sigma Aldrich, St. Louis, MI), an irreversible GLUT1–4 blocker, following 4 × 5 min washing in uptake buffer. The cells were lysed in 1% SDS and added to 3 ml Emulsifier-Safe liquid scintillation cocktail (Perkin-Elmer). Intracellular radioactivity was quantified by liquid scintillation counting using the Packard Tri-Carb 2900 (Perkin-Elmer). As a control, 10 μM indinavir (Sigma Aldrich) (26), a specific GLUT4 inhibitor, was used to determine the GLUT4-specific transport in cultures from TBC1D4<sup>+/+</sup> and TBC1D4<sup>-/-</sup>

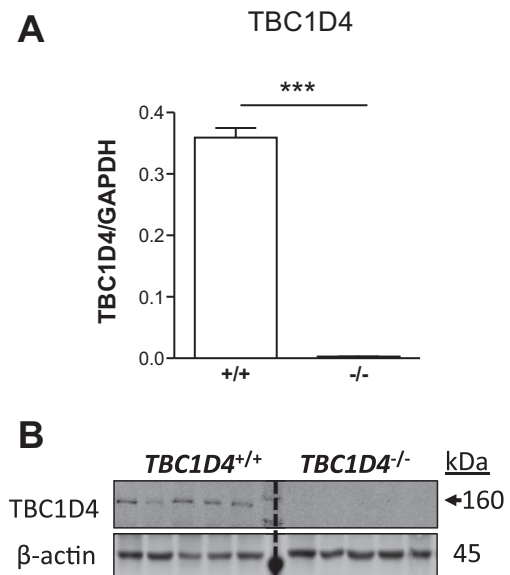


Fig. 1. TBC1D4 mRNA and protein are not detectable in kidneys of TBC1D4-deficient (TBC1D4<sup>-/-</sup>) mice. Detection of TBC1D4 mRNA levels by qRT-PCR (A) and protein abundance by immunoblotting (B) in whole kidney lysates from wild-type (TBC1D4<sup>+/+</sup>) and TBC1D4<sup>-/-</sup> mice. Values are normalized to either GAPDH (mRNA) or β-actin (protein) and expressed as means ± SE,  $n \geq 5$  mice/group. \*\*\* $P < 0.001$ .



mice. Glucose uptake with cytochalasin B served to normalize the values. All values were expressed in picomoles per hour per square centimeter.

**Statistical analyses.** Statistical analyses were performed with the GraphPad Prism Software (San Diego, CA). Data are represented as means  $\pm$  SE and were tested for significance using one- or two-way ANOVA followed by unpaired Student's *t*-test and Bonferroni or false discovery rate (FDR) correction where appropriate.  $P < 0.05$  was considered statistically significant.

## RESULTS

**TBC1D4 deletion does not affect renal salt and water handling.** To investigate the function of TBC1D4 in the kidney, we used constitutive TBC1D4 knockout mice (TBC1D4<sup>-/-</sup>) (35) and compared them with age-matched wild-type TBC1D4<sup>+/+</sup> mice. Quantitative RT-PCR and immunoblotting confirmed the effective deletion of TBC1D4 in the kidneys of TBC1D4<sup>-/-</sup> mice (Fig. 1, A and B). As previously described, TBC1D4<sup>-/-</sup> mice did not reveal any gross abnormalities (31, 35, 57). On standard diet, mice of both genotypes revealed similar body weights, food and water intake, plasma pH and ion (Na<sup>+</sup>, K<sup>+</sup>, Cl<sup>-</sup>) concentrations, as well as plasma aldosterone and corticosterone levels (Table 2). Likewise, urinary volume excretion, osmolarity, and ion excretion (Na<sup>+</sup>, K<sup>+</sup>) did not differ between genotypes. Accordingly, blood pressure measurements using the noninvasive tail-cuff method revealed no difference between TBC1D4<sup>+/+</sup> and TBC1D4<sup>-/-</sup> mice (Table 2).

**TBC1D4 deletion does not affect renal expression of salt- and water-transporting proteins.** To determine if the lack of TBC1D4 affects renal ion-transporting proteins in distal tubule segments, we assessed the abundance of NKCC2, NCC, ENaC, Na<sup>+</sup>-K<sup>+</sup>-ATPase, and AQP2 (Fig. 2). Densitometric analysis did not reveal any significant differences in the protein abundance of NKCC2, NCC, the three ENaC subunits  $\alpha$ ,  $\beta$ ,  $\gamma$ , AQP2, and the Na<sup>+</sup>-K<sup>+</sup>-ATPase between control and

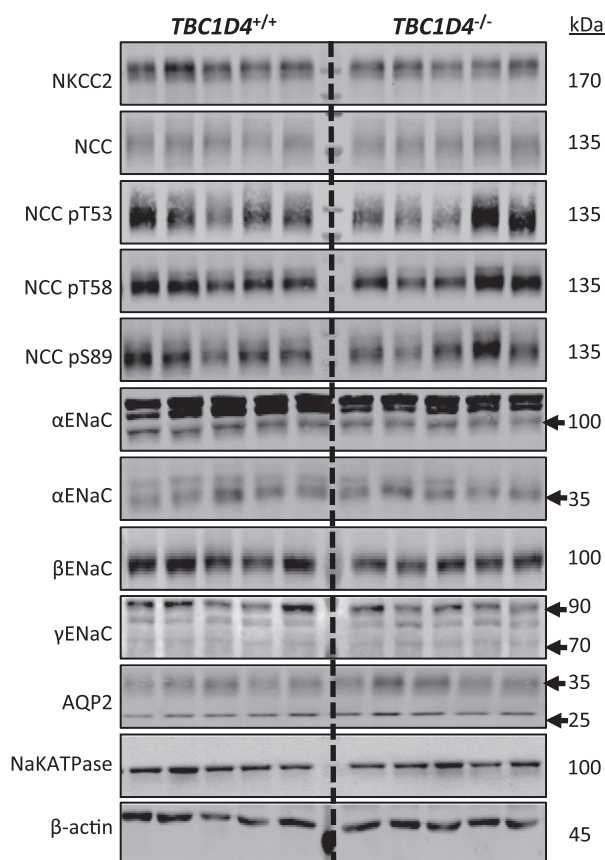


Fig. 2. TBC1D4 deficiency does not affect the abundance and/or phosphorylation of renal Na<sup>+</sup> and water-transporting proteins. Detection by immunoblotting of NKCC2, total NaCl cotransporter (NCC), and NCC phosphorylated at threonine-53 (pT53), threonine-58 (pT58), and serine (pS89),  $\alpha$ -,  $\beta$ -, and  $\gamma$ -epithelial Na<sup>+</sup> channel (ENaC), aquaporin-2 (AQP2), and the Na<sup>+</sup>-K<sup>+</sup>-ATPase in membrane preparation from kidneys of TBC1D4<sup>+/+</sup> and TBC1D4<sup>-/-</sup> mice kept on a standard diet. Detection of  $\beta$ -actin served for normalization of the densitometric data provided in Table 3.

Table 2. Physiological, blood, and urine parameters of TBC1D4<sup>+/+</sup> and TBC1D4<sup>-/-</sup> mice on standard diet

	WT	KO	P Value
<b>Physiology</b>			
SBP, mmHg	100.9 $\pm$ 2.7 (4)	96.3 $\pm$ 4.4 (4)	0.399
Body wt, g	31.9 $\pm$ 2.2 (8)	30.9 $\pm$ 0.7 (7)	0.668
Food intake, mg·g body wt <sup>-1</sup> ·24 h <sup>-1</sup>	109.9 $\pm$ 20.5 (4)	113.7 $\pm$ 26.8 (3)	0.913
Water intake, $\mu$ l·g body wt <sup>-1</sup> ·24 h <sup>-1</sup>	151.7 $\pm$ 39.2 (4)	138.1 $\pm$ 9.2 (3)	0.784
<b>Blood</b>			
pH	7.37 $\pm$ 0.03 (8)	7.36 $\pm$ 0.03 (7)	0.988
Na <sup>+</sup> , mM	148 $\pm$ 0.42 (8)	146.9 $\pm$ 0.40 (7)	0.075
K <sup>+</sup> , mM	4.19 $\pm$ 0.11 (8)	3.87 $\pm$ 0.20 (7)	0.162
Cl <sup>-</sup> , mM	110.1 $\pm$ 1.25 (8)	110.7 $\pm$ 1.34 (7)	0.752
Corticosterone, nM	658.71 $\pm$ 91.25 (7)	811.55 $\pm$ 76.52 (6)	0.235
Aldosterone, nM	0.64 $\pm$ 0.13 (7)	0.86 $\pm$ 0.17 (6)	0.328
Glucose, mM	8.05 $\pm$ 0.45 (14)	8.78 $\pm$ 0.84 (10)	0.418
Insulin, ng/ml	0.40 $\pm$ 0.04 (7)	0.35 $\pm$ 0.01 (7)	0.234
<b>Urine</b>			
Urine excretion, ml/24 h	1.0 $\pm$ 0.2 (18)	1.0 $\pm$ 0.2 (19)	0.936
Osmolarity, mosmol/kgH <sub>2</sub> O	2,993 $\pm$ 205.3 (9)	3,430 $\pm$ 447.9 (9)	0.390
Na <sup>+</sup> (norm. to Creat.)	21.91 $\pm$ 2.61 (23)	23.93 $\pm$ 3.95 (20)	0.618
K <sup>+</sup> (norm. to Creat.)	52.97 $\pm$ 6.37 (23)	54.39 $\pm$ 6.49 (20)	0.879
Ratio Na <sup>+</sup> /K <sup>+</sup>	0.45 $\pm$ 0.04 (23)	0.46 $\pm$ 0.04 (20)	0.839
Aldosterone, ng/24 h	13.36 $\pm$ 4.31 (7)	13.30 $\pm$ 4.46 (6)	0.957

Values are mean  $\pm$  SE. WT, wild type; KO, knockout; Creat, creatinine. Statistical differences between TBC1D4<sup>+/+</sup> and TBC1D4<sup>-/-</sup> mice were assessed by unpaired *t*-test.

TBC1D4<sup>-/-</sup> mice (Table 3). Moreover, using phosphospecific antibodies, we did not obtain any evidence that the phosphorylation of NCC at the positions T53, T58, and S89 was changed. Phosphorylation of NCC at these sites were shown to correlate with NCC activity (52).

**TBC1D4 deletion is not compensated by an increased expression of TBC1D1 or other TBC1D proteins.** TBC1D1 is a close homolog of TBC1D4 that has similar Akt phosphorylation sites and does also regulate GLUT4 trafficking (11, 48). Interestingly, TBC1D1 is also highly expressed in the kidney (14). Therefore, we next tested whether the lack of TBC1D4 might be compensated by an altered expression of TBC1D1. However, we could not find any modulation in renal TBC1D1 protein abundance between TBC1D4<sup>+/+</sup> and TBC1D4<sup>-/-</sup> mice (Fig. 3). Consistent with this observation, preliminary experiments in TBC1D4/TBC1D1 double-knockout mice (13) did not reveal any evidence for an altered renal salt and water handling in these mice. Furthermore, we performed microarray analyses on COPAS-isolated DCTs of TBC1D4<sup>+/+</sup> and TBC1D4<sup>-/-</sup> mice to check whether other members of the TBC1 protein family might be upregulated in response to TBC1D4 deficiency. Because DCTs were shown to have a very high TBC1D4 protein abundance (35), we expected that a

Table 3. Summary of densitometric analyses performed on immunoblots of kidneys from *TBC1D4*<sup>+/+</sup> and *TBC1D4*<sup>-/-</sup> mice kept either on standard diet or LNa/HKD

	Standard Diet			LNa/HK		
	WT	KO	P value	WT	KO	P value
NKCC2	100 ± 7.4	100 ± 14.8	0.999	100 ± 8.9	74.5 ± 12.4	0.132
tNCC	100 ± 12.3	113.0 ± 14.4	0.506	100 ± 27.1	65.5 ± 19.2	0.329
NCC pT53	100 ± 12.0	114.7 ± 14.0	0.439	100 ± 24.7	62.7 ± 13.4	0.221
NCC pT58	100 ± 5.8	107.9 ± 17.8	0.68	100 ± 18.4	125.6 ± 28.1	0.467
NCC pS89	100 ± 9.9	113.3 ± 18.2	0.534	100 ± 15.5	118.3 ± 19.2	0.480
α-ENaC (90 kDa)	100 ± 8.7	91.5 ± 13.5	0.606	100 ± 22.9	115.1 ± 27.2	0.703
α-ENaC (35 kDa)	100 ± 13.7	107.4 ± 12.8	0.700	100 ± 34.7	116.4 ± 17.4	0.668
β-ENaC	100 ± 12.9	103.7 ± 23.6	0.893	100 ± 11.9	98.9 ± 13.6	0.950
γ-ENaC (90 kDa)	100 ± 8.4	125.6 ± 13.5	0.133	100 ± 11.5	103.2 ± 10.7	0.844
γ-ENaC (70 kDa)	100 ± 11.1	110.8 ± 7.4	0.434	100 ± 15.5	99.3 ± 12.7	0.973
AQP2 (35 kDa)	100 ± 16.4	122.6 ± 14.0	0.314	100 ± 9.9	82.7 ± 10.7	0.268
AQP2 (25 kDa)	100 ± 16.1	105.0 ± 7.0	0.781	100 ± 15.4	80.3 ± 13.9	0.370
Na <sup>+</sup> -K <sup>+</sup> -ATPase	100 ± 13.0	110.1 ± 4.1	0.471	100 ± 4.4	93.3 ± 3.4	0.264
TBC1D1	100 ± 4.8	94.0 ± 14.6	0.706	100 ± 8.8	77.7 ± 16.1	0.260
AKT	100 ± 9.4	139.7 ± 23.4	0.141	100 ± 8.3	107.6 ± 6.2	0.483
pAKT (S473)	100 ± 3.6	100.7 ± 15.6	0.961	100 ± 22.9	188 ± 32.6	0.057
ERK1/2	100 ± 9.1	104.4 ± 2.5	0.650	100 ± 5.3	103.6 ± 5.8	0.660
pERK1/2	100 ± 10.2	131.7 ± 16.1	0.134			
GLUT4 (S)	100 ± 8.4	71.4 ± 7.2 *	0.024	100 ± 12.5	63.4 ± 7.2 *	0.034
GLUT4 (M)	100 ± 10.3	70.2 ± 6.5 *	0.029	100 ± 13.5	61.0 ± 7.3 *	0.035

All values were normalized to β-actin and expressed as means ± SE; *n* ≥ 5 mice/group. LNa/HK, low Na<sup>+</sup>/high K<sup>+</sup>; S and M indicate the GLUT4 antibodies from Sigma-Aldrich and Millipore, respectively. \**P* < 0.05.

differential regulation of gene products between *TBC1D4*<sup>+/+</sup> and *TBC1D4*<sup>-/-</sup> mice might be most prominent in this segment. However, although the microarray data confirmed the loss of *TBC1D4* expression, they did not reveal any significant differential regulation for all analyzed gene products of the *TBC1D* family (Table 4).

*TBC1D4* is dispensable for the renal adaptation to a LNa/HKD or water restriction. Previous in vitro data had suggested that *TBC1D4* is involved in the aldosterone- and vasopressin-dependent regulation of ENaC and AQP2, respectively (27, 29, 34). Therefore, we next tested whether the *TBC1D4*<sup>-/-</sup> mice may show a defect in urinary ion and water excretion and/or the expression of ENaC and AQP2 when challenged by conditions known to increase endogenous aldosterone and vasopressin production. First, we fed mice with a LNa (<0.03%)/HKD (5%) to maximally stimulate the renin-angiotensin-aldosterone system (RAAS). Similar to standard diet, no difference between *TBC1D4*<sup>+/+</sup> and *TBC1D4*<sup>-/-</sup> mice was detected concerning urinary ion and hormone excretion and plasma hormone levels (Table 5). Likewise, the protein abundances of NKCC2, NCC (total and pT53, pT58, and pS89), ENaC, AQP2, and Na<sup>+</sup>-K<sup>+</sup>-ATPase were similar between

*TBC1D4*<sup>+/+</sup> and *TBC1D4*<sup>-/-</sup> mice even on LNa/HKD (Fig. 4 and Table 3). Finally, we analyzed whether *TBC1D4*<sup>-/-</sup> mice were able to concentrate urine during water restriction. To avoid a maximum activation of compensatory mechanisms that may mask subtle effects of the gene deletion on urinary ion excretion, we chose a previously described protocol with a mild but not complete water deprivation (59). The drinking bottle with tap water was removed, but water was added to the dry chow as described in MATERIALS AND METHODS. Compared with the period of ad libitum water access, the food intake slightly increased (Fig. 5A), whereas the urine volumes significantly dropped during the water restriction period (Fig. 5B). Urine osmolarity (Fig. 5C), water balance (Fig. 5D), urinary cation excretion (Na<sup>+</sup>, K<sup>+</sup>, Mg<sup>2+</sup>) (Fig. 5E), and the Na<sup>+</sup>-to-K<sup>+</sup> ratio did not differ between the genotypes. Likewise, urinary aldosterone levels were similar in *TBC1D4*<sup>+/+</sup> and *TBC1D4*<sup>-/-</sup> mice (Fig. 5F).

*TBC1D4* colocalizes with GLUT4 along the nephron and regulates its expression. *TBC1D4* is coexpressed with and regulates GLUT4 in classical (fat and muscle) (10, 28) and nonclassical (heart and pancreas) insulin-responsive tissues (8, 57). Previous studies reported also *TBC1D4* and GLUT4

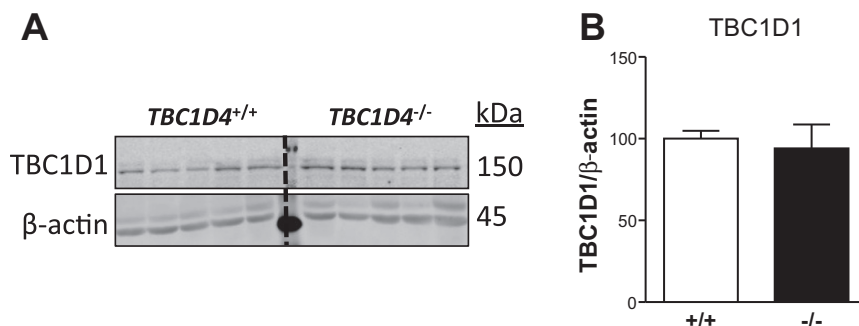


Fig. 3. *TBC1D4* deficiency does not induce increased abundance of the close homolog *TBC1D1*. A: detection by immunoblotting of *TBC1D1* in whole kidney lysates from *TBC1D4*<sup>+/+</sup> and *TBC1D4*<sup>-/-</sup> mice kept on a standard diet. B: detection of β-actin served for normalization of the densitometric data shown as bar graphs. Open bar, *TBC1D4*<sup>+/+</sup> mice; filled bar, *TBC1D4*<sup>-/-</sup>. All values are means ± SE, *n* = 5 mice/group.

Table 4. Microarray analysis of mRNA expression levels of TBC1D family members in COPAS-isolated DCTs of TBC1D4<sup>+/+</sup> and TBC1D4<sup>-/-</sup> mice

Gene	WT	KO	Overall FDR Corrected	Selected FDR Corrected
TBC1D1	6.81 ± 0.05	6.83 ± 0.03	1	0.982
TBC1D2	4.85 ± 0.11	4.86 ± 0.07	1	0.982
TBC1D2B	4.81 ± 0.09	4.86 ± 0.09	1	0.982
TBC1D4	6.75 ± 0.07	2.47 ± 0.11	9.15 <sup>-8*</sup>	1.82 <sup>-6*</sup>
TBC1D5	5.37 ± 0.04	5.32 ± 0.03	1	0.982
TBC1D7	6.52 ± 0.05	6.48 ± 0.06	1	0.982
TBC1D8	4.16 ± 0.12	4.17 ± 0.01	1	0.982
TBC1D8B	5.8 ± 0.02	5.91 ± 0.05	1	0.529
TBC1D9	5.64 ± 0.02	5.69 ± 0.03	1	0.808
TBC1D9B	6.71 ± 0.03	6.73 ± 0.06	1	0.982
TBC1D10A	4.67 ± 0.06	4.87 ± 0.07	1	0.584
TBC1D10B	4.85 ± 0.06	4.89 ± 0.04	1	0.982
TBC1D10C	2.99 ± 0.08	3.01 ± 0.11	1	0.982
TBC1D12	6.24 ± 0.04	6.11 ± 0.08	1	0.808
TBC1D13	6.67 ± 0.08	6.66 ± 0.04	1	0.982
TBC1D14	7.58 ± 0.05	7.60 ± 0.03	1	0.982
TBC1D15	5.94 ± 0.08	5.93 ± 0.10	1	0.982
TBC1D16	4.37 ± 0.13	4.18 ± 0.06	1	0.808
TBC1D17	5.57 ± 0.08	5.54 ± 0.07	1	0.982
TBC1D19	7.16 ± 0.05	7.14 ± 0.06	1	0.982
TBC1D20	6.42 ± 0.07	6.42 ± 0.01	1	0.982
TBC1D21	1.84 ± 0.04	1.86 ± 0.05	1	0.982
TBC1D22A	5.14 ± 0.07	5.18 ± 0.05	1	0.982
TBC1D22B	6.64 ± 0.04	6.50 ± 0.07	1	0.775
TBC1D23	5.45 ± 0.06	5.28 ± 0.03	1	0.456
TBC1D24	5.93 ± 0.07	5.86 ± 0.04	1	0.982
TBC1D25	5.59 ± 0.04	5.59 ± 0.05	1	0.982
TBC1D30	2.81 ± 0.08	2.85 ± 0.04	1	0.982

Values are means ± SE; *n* = 4 mice/group. COPAS, complex object parametric analysis and sorting; DCT, distal convoluted tubule; FDR, false discovery rate. After FDR correction of selected TBC1D genes (*n* = 28), only TBC1D4 resulted as differentially regulated mRNA in DCTs of TBC1D4<sup>-/-</sup> mice. \**P* < 0.0017.

expression in the kidney (2, 5, 9, 15, 35). Therefore, we aimed at determining whether TBC1D4 colocalizes with GLUT4 in renal epithelial cells and whether the expression of the transporter is affected in TBC1D4<sup>-/-</sup> mice as reported for skeletal muscle and adipose cells (13, 31, 57). We first analyzed the

Table 5. Physiological, blood, and urine parameters of TBC1D4<sup>+/+</sup> and TBC1D4<sup>-/-</sup> mice on LNa/HKD

	<sup>+/+</sup> ( <i>n</i> = 5)	<sup>-/-</sup> ( <i>n</i> = 5)	<i>P</i> Value
Physiology			
Body wt, g	22.0 ± 0.3	22.2 ± 0.7	0.778
Food intake, mg·g body wt <sup>-1</sup> ·24 h <sup>-1</sup>	234.9 ± 24.8	217.8 ± 15.0	0.570
Water intake, μl·g body wt <sup>-1</sup> ·24 h <sup>-1</sup>	348.7 ± 43.4	298.1 ± 18.7	0.316
Renin mRNA levels, arbitrary units	0.27 ± 0.0	0.28 ± 0.1	0.827
Blood			
Corticosterone, nM	304.41 ± 26.70	416.15 ± 59.98	0.127
Aldosterone, nM	5.24 ± 1.05	5.15 ± 1.45	0.96
Glucose, mM	7.08 ± 0.56	5.3 ± 0.34	0.026
Insulin, ng/ml	0.66 ± 0.07	0.55 ± 0.06	0.253
Urine			
Urine excretion, ml/24 h	4.1 ± 0.8	3.3 ± 0.7	0.357
Osmolarity, mosmol/kgH <sub>2</sub> O	3,090 ± 491.3	3,274 ± 305.3	0.759
Na <sup>+</sup> (normal. to Creat.)	5.28 ± 0.74	5.61 ± 0.43	0.713
K <sup>+</sup> (normal. to Creat.)	894.31 ± 68.64	909.04 ± 94.25	0.903
Ratio Na <sup>+</sup> /K <sup>+</sup>	0.006 ± 0.00	0.007 ± 0.00	0.622
Aldosterone, ng/24 h	373.09 ± 51.29	353.88 ± 64.80	0.819

Values are means ± SE. Statistical differences between TBC1D4<sup>+/+</sup> and TBC1D4<sup>-/-</sup> mice were assessed by unpaired *t*-test.

localization of GLUT4 mRNA expression along the nephron and correlated it with TBC1D4 expression data. GLUT4 mRNA levels in microdissected tubules showed the highest expression in the TAL (Fig. 6A); therefore, the TAL was used as reference segment (100%). We found that GLUT4 expression was low in proximal segments (~10%) and in the glomerulus (~20%), intermediate in the CNT/CD (~41%), and high in the DCT (~74%) (Fig. 6A). TBC1D4 mRNA showed a similar distribution (Fig. 6B). Immunostainings for GLUT4 and nephron segment-specific marker molecules on consecutive cryosections confirmed GLUT4 abundance in NKCC2-positive medullary and cortical TAL, NCC-positive DCT, and AQP2-positive CNT/CD (Fig. 6C). Moreover, we analyzed renal GLUT4 abundance by immunoblotting using membrane fractions. As shown in Fig. 6D, TBC1D4<sup>-/-</sup> mice displayed a significant reduction of ~30% of GLUT4 protein expression levels. This reduction of GLUT4 abundance in TBC1D4<sup>-/-</sup> mice was confirmed with a second GLUT4 antibody (data not shown) and by immunohistochemistry (IHC) (Fig. 6E). Renal GLUT4 mRNA levels did not differ between the genotypes (Fig. 6F), pointing to a posttranslational regulation of GLUT4 abundance. Overall, these data suggested that TBC1D4 is an important regulator of GLUT4 in renal epithelial cells, as evidenced by its colocalization and the reduction of GLUT4 expression in TBC1D4<sup>-/-</sup> mouse kidney.

**TBC1D4 deletion increases basal glucose uptake in primary TAL cells.** To investigate the functional impact of TBC1D4 on glucose uptake in renal distal tubule epithelial cells, we isolated and grew primary TAL cells as previously described (22).



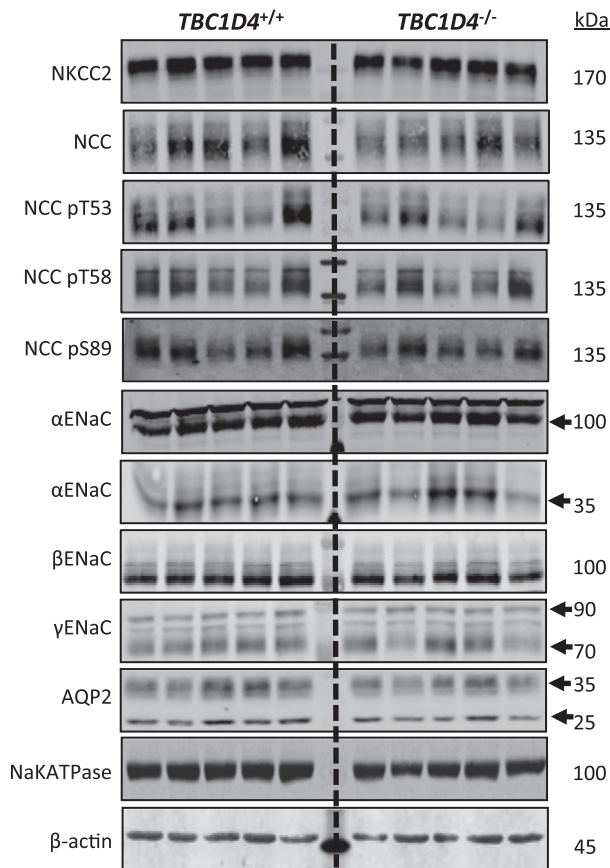


Fig. 4. Challenging  $TBC1D4^{+/+}$  and  $TBC1D4^{-/-}$  mice with a low  $Na^+$ /high- $K^+$  diet does not provoke any differences in the abundance and/or phosphorylation of renal  $Na^+$  and water-transporting proteins between genotypes. Detection by immunoblotting of NKCC2, total NCC, and NCC T53, pT58, and pS89,  $\alpha$ -,  $\beta$ -, and  $\gamma$ -ENaC, AQP2, and the  $Na^+$ - $K^+$ -ATPase in membrane preparation from kidneys of  $TBC1D4^{+/+}$  and  $TBC1D4^{-/-}$  mice kept for 10 days on a low  $Na^+$  ( $<0.03\%$ ), high  $K^+$  ( $5.0\%$ ) diet. Detection of  $\beta$ -actin served for normalization of the densitometric data provided in Table 3.

TAL cell culture was chosen because the RT-PCR data indicated that TAL cells express the highest GLUT4 levels of all distal tubule segments and because the previously established cell culture protocols ensured sufficient polarized and well-differentiated cells for functional analysis. Although the total protein abundance of GLUT4 was reduced in the kidneys of  $TBC1D4^{-/-}$  mice, we found that glucose uptake under basal conditions was significantly higher in TAL cells of  $TBC1D4^{-/-}$  compared with  $TBC1D4^{+/+}$  mice (Fig. 7A). Furthermore, insulin-induced glucose uptake, which was well observed in  $TBC1D4^{+/+}$  cells, was completely abrogated in the  $TBC1D4^{-/-}$  TAL cells (Fig. 7A). To determine the fraction of GLUT4-mediated glucose uptake in response to insulin, we treated the cells with indinavir, a reversible blocker of GLUT4. Costimulation of insulin and indinavir abolished the insulin stimulatory effects in wild-type and restored the glucose uptake of  $TBC1D4^{-/-}$  cells to normal (Fig. 7A). This suggested that the higher glucose uptake observed in  $TBC1D4^{-/-}$  cells under basal condition was due to an impaired GLUT4 regulation. To reveal a potential dysfunction of insulin signaling in  $TBC1D4^{-/-}$  mice kidney, we analyzed the insulin receptor expression. As shown in Fig. 7B,  $TBC1D4^{-/-}$  mice presented similar mRNA levels of the insulin receptor as  $TBC1D4^{+/+}$

mice. Furthermore, the downstream effectors of insulin signaling, Akt and ERK1/2, were not differentially abundant and/or phosphorylated between  $TBC1D4^{+/+}$  and  $TBC1D4^{-/-}$  mice (Fig. 7C). These data suggested that the dysregulation of glucose uptake in  $TBC1D4$ -deficient TAL cells was not due to alterations in insulin signaling upstream of  $TBC1D4$ . These data were further supported by the microarray data that did not provide any evidence for a differential regulation of mRNAs encoding for proteins involved in glucose transport and/or insulin signaling.

## DISCUSSION

With the use of a  $TBC1D4$ -deficient mouse model, this study evaluated the physiological significance of the Rab-GAP  $TBC1D4$  in the kidney. In contrast to evidence from previous *in vitro* data, our findings did not support the idea that  $TBC1D4$  is crucial for the physiological regulation of renal  $Na^+$  and water handling. However, our findings provide clear evidence that  $TBC1D4$  controls GLUT4-mediated glucose uptake in renal distal tubules, which points to a hitherto not assumed role of  $TBC1D4$  in the kidney.

In a mouse cortical collecting duct cell line,  $TBC1D4$  knockdown increases amiloride-sensitive  $Na^+$  currents and the cell surface abundance of ENaC (34). Likewise,  $TBC1D4$  was shown to interact with the  $\alpha$ -subunit of the  $Na^+$ - $K^+$ -ATPase and to retain the pump at intracellular sites in heterologous expression systems (3). Taken together, these findings suggest that  $TBC1D4$  may decrease tubular  $Na^+$  reabsorption. Conversely, the deletion of  $TBC1D4$  may cause ENaC-dependent renal  $Na^+$  retention and may eventually increase blood pressure as observed in humans and mouse models with ENaC hyperactivity (42, 51). Surprisingly, we did not find any evidence for an altered renal  $Na^+$  transport in  $TBC1D4^{-/-}$  mice.  $TBC1D4^{-/-}$  mice had the same body weight, food and water intake, as well as urinary  $Na^+$  and  $K^+$  excretion and arterial blood pressure as  $TBC1D4^{+/+}$  mice.  $TBC1D4^{-/-}$  mice did not even reveal any difference in phenotype compared with  $TBC1D4^{+/+}$  mice when challenged by a LNa/HKD, which is supposed to maximally increase endogenous aldosterone production. This contrasts with constitutive or kidney-specific *Nedd4-2* and *SGK1* knockout mouse models, which show an overt renal transport defect with altered arterial blood pressure as soon as they are challenged by an altered dietary salt intake (19, 46).

Urine concentration critically depends on vasopressin-dependent water reabsorption via apical AQP2 water channels in the renal collecting system. Deficits in vasopressin-dependent signaling and AQP2 regulation are associated with severe defects in renal water handling as has been observed in patients and in mouse models (30, 45). In *mpkCCD* cells, the knockdown of  $TBC1D4$  cells was shown to increase the cell surface abundance of the water channel AQP2, suggesting that  $TBC1D4$  may contribute to the control of renal water handling (27, 29). However, in line with the results on renal  $Na^+$  uptake, we were unable to provide any evidence that the loss of  $TBC1D4$  *in vivo* influences the regulation of renal water reabsorption and/or of AQP2. Compared with  $TBC1D4^{+/+}$  mice, the  $TBC1D4^{-/-}$  mice did not show any difference in urine concentration or AQP2 abundance, neither under standard conditions nor in response to water restriction.

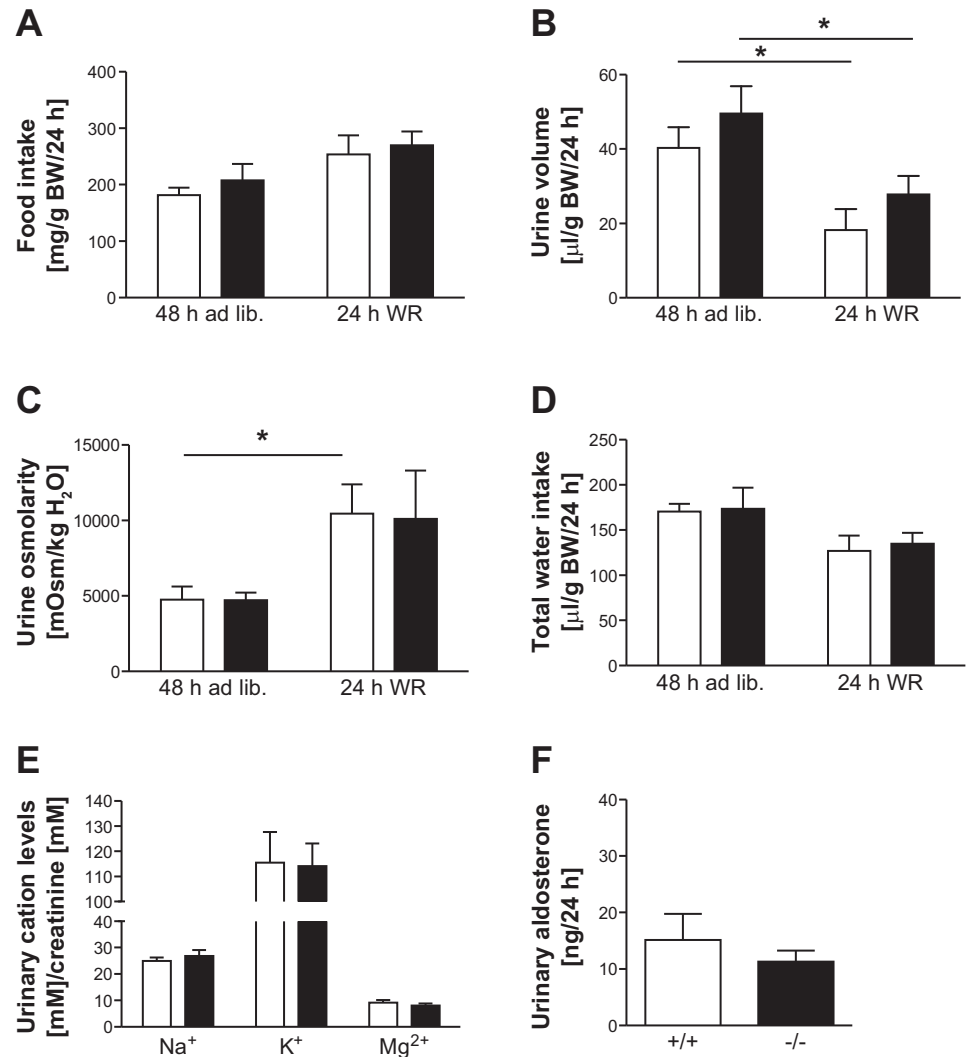


Fig. 5. TBC1D4 deficiency does not impair the renal adaptation to water restriction (WR). Response of TBC1D4<sup>+/+</sup> (open bars) and TBC1D4<sup>-/-</sup> (filled bars) mice to 48-h ad libitum (ad lib.) access to water and to 24-h mild water restriction as described in MATERIALS AND METHODS. Mice were kept in metabolic cages to record food intake (A), urine volume (B), urine osmolarity (C), total water intake (D), urinary cation concentration normalized to urinary creatinine concentrations (E), and urinary aldosterone excretion (F). Total water intake was calculated from water intake and water content in the food. All values are means  $\pm$  SE;  $n \geq 5$  mice/group. \* $P < 0.05$ .

Taking into account previous in vitro findings that suggest a strong role of TBC1D4 in the regulation of ENaC, Na<sup>+</sup>-K<sup>+</sup>-ATPase, and AQP2 (3, 27, 29, 34), our findings are surprising. In skeletal muscle cells, other members of the TBC1D protein family such as TBC1D1 have overlapping functions with TBC1D4 and contribute to the regulation of GLUT4 (11, 13). This may account for a reciprocal compensation between these two proteins or even across the entire Rab-GAP TBC1D protein family. However, using immunoblotting for TBC1D1 and microarray analyses, we did not detect any evidence that the loss of TBC1D4 is compensated by the upregulation of any of the TBC1D proteins (Table 4) and/or any other mRNA involved in protein trafficking, renal ion and water transport, as well as glucose metabolism. Thus, although we cannot completely exclude the activation of compensatory mechanisms in the TBC1D4 knockout mice, our study indicates that TBC1D4 is dispensable for the physiological regulation of ENaC, Na<sup>+</sup>-K<sup>+</sup>-ATPase, and AQP2 in the kidney in vivo.

In the kidney, GLUT4 expression has been documented in renal vessels (9), glomeruli, the TAL (9, 15), proximal and distal tubules (2), and in juxtaglomerular cells (5). However, the reported expression patterns varied between studies, which may be explained by the use of different probes and that either

mRNA or protein expressions were analyzed. Here, we combined qRT-PCR analysis on microdissected tubule segments with IHC studies to establish a detailed description of GLUT4 abundance along the nephron. With the use of two different GLUT4 antibodies, GLUT4 was found to be highly abundant along the entire distal nephron, whereas proximal tubules and glomeruli expressed very little, if any, GLUT4. The predominant localization of GLUT4 along the distal nephron matches with the capability of the distal tubules for anaerobic glycolysis, which requires substantial glucose uptake into the cells (23, 47). In fact, although the proximal tubules depend mainly on aerobic metabolism, the distal tubules possess a high anaerobic capacity (6, 25) and express the necessary glycolytic enzymes such as hexokinase, pyruvate kinase, phosphofructokinase (23), insulin receptors, insulin-like receptors, and downstream signaling pathways, including insulin receptor substrate, and PKB/Akt (12, 32, 43). Furthermore, the renal distal tubules have a high epithelial transport activity, which is reflected in a high mitochondrial density and strong expression of the Na<sup>+</sup>-K<sup>+</sup>-ATPase (44). Thus, GLUT4-dependent glucose uptake may fuel the high energy demand of distal tubules. Interestingly, vasopressin and other cAMP-increasing hormones were also shown to regulate GLUT4 phosphorylation in medullary



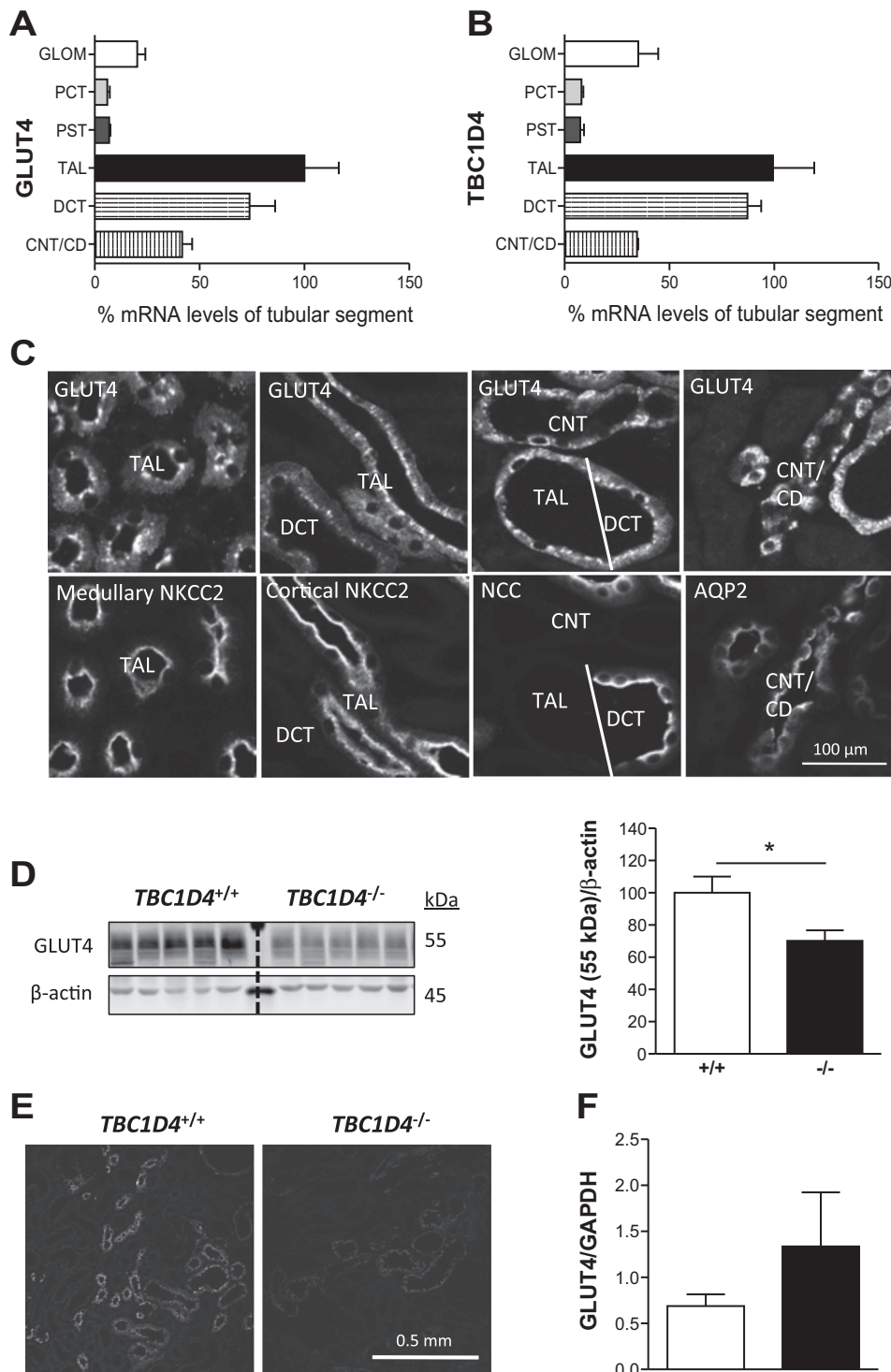


Fig. 6. TBC1D4 and GLUT4 colocalize along the distal nephron, and TBC1D4 deficiency reduces renal GLUT4 protein abundance. Expression levels of GLUT4 mRNA (A) and TBC1D4 mRNA (B) in microdissected glomeruli and tubule segments of TBC1D4<sup>+/+</sup> mice. The mRNA levels were analyzed by qRT-PCR, normalized to GAPDH mRNA expression levels, and then expressed in percent of the expression levels in the segment with the highest expression levels [thick ascending limb (TAL)]. Values are means  $\pm$  SE,  $n \geq 3$  mice for each segment. C: immunohistochemical detection of either GLUT4 (top) or NKCC2, NCC, and AQP2 (bottom) in consecutive cryosections of the renal cortex and medulla of wild-type mice. GLUT4 is found in the NKCC2-positive medullary and cortical TAL, NCC-positive distal convoluted tubule (DCT), and AQP2-positive connecting tubule (CNT)/collecting duct (CD). D: detection by immunoblotting of GLUT4 (Millipore) in membrane preparation from kidneys of TBC1D4<sup>+/+</sup> and TBC1D4<sup>-/-</sup> mice kept on a standard diet. Detection of  $\beta$ -actin served for normalization of the densitometric data provided in the corresponding bar graph and in Table 3. Values are means  $\pm$  SE;  $n = 5$  mice/group, \* $P < 0.05$ . E: immunohistochemical detection of GLUT4 (Millipore) in renal cortex of a TBC1D4<sup>+/+</sup> and a TBC1D4<sup>-/-</sup> mouse; presented images are representative for all analyzed mice ( $n > 3$ /group). F: quantitative analysis by qRT-PCR of GLUT4 mRNA levels in kidneys of TBC1D4<sup>+/+</sup> and a TBC1D4<sup>-/-</sup> mice. Values are normalized to GAPDH mRNA levels and expressed as means  $\pm$  SE;  $n \geq 5$  mice/group.

TALs, suggesting a concerted regulation of ion transport and glucose uptake (24).

Consistent with numerous previous studies on muscle cells and adipocytes (33, 49), our IHC experiments showed a predominant intracellular localization of GLUT4. However, they did not allow a clear apical and/or basolateral plasma membrane localization. Nevertheless, given that the proximal tubules recover most of the filtered glucose from the urine and

that therefore the tubular fluid at distal tubules is usually glucose free, it is reasonable to assume that glucose uptake by GLUT4 can only be achieved via the basolateral cell side. Future studies will need to address this in more detail. These studies may also determine whether GLUT4 translocates from intracellular sites to the cell surface in response to insulin, as it was shown in adipocytes and skeletal muscle cells (13, 31, 57). Our experiments further demonstrated a strong correlation

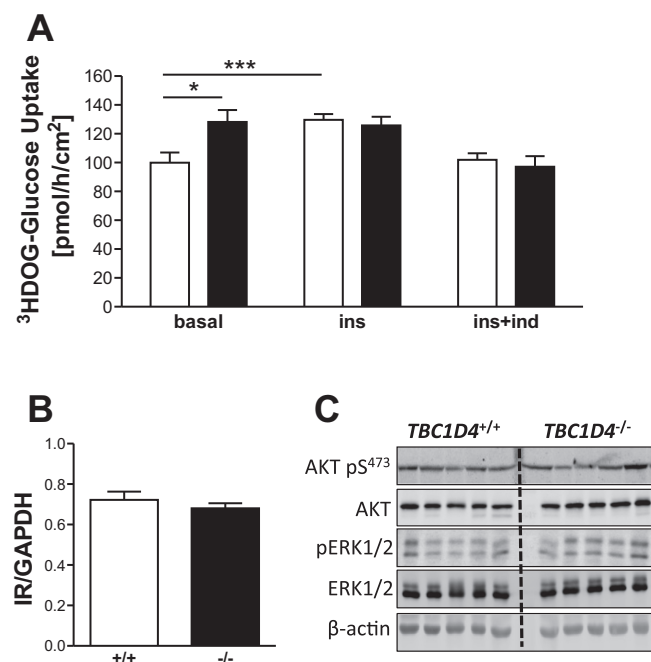


Fig. 7. TBC1D4 deficiency increases basal glucose uptake but abrogates insulin-stimulated glucose uptake in TAL cells. **A**: analysis of basal and insulin-stimulated 2-[<sup>3</sup>H]deoxyglucose (<sup>3</sup>HDOG-glucose) uptake in primary TAL cell cultures isolated from TBC1D4<sup>+/+</sup> (open bars) and TBC1D4<sup>-/-</sup> (filled bars) mice. Insulin (300 nM) was applied for 15 min either alone (ins) or together with the specific GLUT4 inhibitor indinavir (ind, 10  $\mu$ M). Values are means  $\pm$  SE;  $n \geq 3$  cell cultures/group. \* $P < 0.05$  and \*\*\* $P < 0.001$ . **B**: quantitative analysis by qRT-PCR of insulin receptor (IR) mRNA levels in kidneys of TBC1D4<sup>+/+</sup> and TBC1D4<sup>-/-</sup> mice. Values are normalized to GAPDH mRNA levels and expressed as means  $\pm$  SE;  $n \geq 5$  mice/group. **C**: detection by immunoblotting of AKT, AKT pS<sup>473</sup>, ERK1/2, and pERK1/2 in whole kidney lysates from TBC1D4<sup>+/+</sup> and TBC1D4<sup>-/-</sup> mice kept on a standard diet. Detection of  $\beta$ -actin served for normalization of the densitometric data provided in Table 3.

between GLUT4 and TBC1D4 abundance along the nephron, indicating a possible functional interaction of both proteins not only in fat and skeletal muscle (18, 55) but also in the kidney. In line with these findings, we were able to convey that renal GLUT4 abundance and glucose uptake in distal tubular epithelial cells depend on TBC1D4. Indeed, renal GLUT4 abundance was reduced in TBC1D4<sup>-/-</sup> mice. This reduction occurred at the protein and not at the mRNA level, suggesting an increased posttranslational protein turnover, similar to what has been described in adipocytes and/or skeletal muscle cells of TBC1D4<sup>-/-</sup> mice (13, 31, 57). Surprisingly, this decrease in GLUT4 protein abundance was not reflected in a reduction of GLUT4-dependent glucose uptake in distal tubule cells. In fact, isolated primary TAL cells of TBC1D4<sup>-/-</sup> mice even showed a higher basal glucose uptake than TAL cells of TBC1D4<sup>+/+</sup> mice, which could not be further stimulated with insulin. Intriguingly, increased GLUT4-mediated glucose uptake, despite reduced total GLUT4 protein levels, was consistently observed also in white fat cells of TBC1D4<sup>-/-</sup> mice although the effect on skeletal muscle cells was more variable (13, 31, 57). The underlying mechanism for the inverse regulation of GLUT4 protein abundance and GLUT4 activity in adipocytes and renal epithelia and the apparent cell type specificity are unclear but may include a differential regulation of GLUT4 protein synthesis and/or turnover, cell surface targeting, and/or

the intrinsic activity of the transporter as discussed by Lansey et al. (31).

What might be the functional consequence of the increased basal GLUT4-dependent glucose uptake in distal tubular epithelial cells? First of all, it may contribute to the altered systemic glucose handling in this (13) and other (31, 57) TBC1D4<sup>-/-</sup> mouse models and in humans with TBC1D4 mutations (17, 40), which was formerly only attributed to the classical insulin-target tissues such as fat and skeletal muscle (13, 57). Likewise, the abrogated response of TBC1D4-deficient TAL cells supports the hypothesis that the observed systemic insulin resistance in TBC1D4<sup>-/-</sup> mice (13, 31, 57) could be partially related to the kidney. Aside from these systemic metabolic effects, the loss of TBC1D4 may improve basolateral glucose uptake and, with that, the glycolytic capacity of distal tubules, which may in turn contribute to their decreased vulnerability during renal ischemia compared with proximal tubules (25). In fact, recent studies showed a decreased intracellular retention of the Na<sup>+</sup>-K<sup>+</sup>-ATPase in distal tubules of TBC1D4<sup>-/-</sup> mice in response to renal ischemia. The effect was attributed to a loss of a direct intracellular retention of the Na<sup>+</sup>-K<sup>+</sup>-ATPase by TBC1D4. However, improved GLUT4-dependent glucose uptake and hence energization of the cells may have also contributed to an improved cell surface targeting of the Na<sup>+</sup>-K<sup>+</sup>-ATPase. Consistent with this idea, the distal tubules of TBC1D4<sup>-/-</sup> mice showed a lower ischemia-induced apoptosis rate than those of TBC1D4<sup>+/+</sup> mice, although the effect did not reach statistical significance (4). The availability of transgenic mice with “floxed” GLUT4 alleles (1) may allow the testing of the role of GLUT4 in distal tubules in systemic glucose handling as well as in their known ischemic tolerance (25).

In conclusion, the disruption of the TBC1D4 gene in mice neither significantly affects the renal control of salt and water homeostasis and blood pressure, nor the abundance of ENaC, AQP2, and the Na<sup>+</sup>-K<sup>+</sup>-ATPase in the kidney. These findings are in contrast to what has previously been suggested based on studies on cells in vitro. Nevertheless, TBC1D4<sup>-/-</sup> mice do have a distinct renal phenotype. Specifically, TBC1D4 deficiency is associated with an increased GLUT4-dependent glucose uptake in distal tubule cells under baseline conditions, which may improve their energy supply and anaerobic glycolytic capacities and may become relevant during renal hypoxia and/or during enhanced tubular workloads.

#### ACKNOWLEDGMENTS

We thank Claudia Sündermann, Monique Carrel, Michèle Heidemeyer, and Udo Schnitzbauer for technical assistance with COPAS sorting, tissue processing, and urine and plasma analysis, respectively. We also thank Drs. Hannah Monyer and Eric Feraille for providing the PV-EGFP mice and the Na<sup>+</sup>-K<sup>+</sup>-ATPase antibody, respectively. We also acknowledge the technical help by the Zurich Integrative Rodent Physiology facility, the Centre for Microscopy and Image Analysis, and the Functional Genomics Centre Zurich.

#### GRANTS

This study was supported by grants from the Swiss National Science Foundation (310030\_143929/1), the Novartis Foundation, and the Zurich Center of Integrative Human Physiology. The laboratories of J. Loffing, N. Faresse, O. Devuyst, and A. Odermatt are also supported by the National Center of Competence in Research Kidney.CH.

#### DISCLOSURES

No conflicts of interest, financial or otherwise, are declared by the authors.

## AUTHOR CONTRIBUTIONS

Author contributions: M.D.C., B.G., D.L.-C., and A.O. performed experiments; M.D.C., B.G., D.L.-C., A.O., O.D., N.F., and J.L. analyzed data; M.D.C., B.G., D.L.-C., A.O., H.A.-H., O.D., N.F., and J.L. interpreted results of experiments; M.D.C. and B.G. prepared figures; M.D.C. and N.F. drafted manuscript; M.D.C., B.G., D.L.-C., A.O., H.A.-H., O.D., N.F., and J.L. approved final version of manuscript; H.A.-H., N.F., and J.L. edited and revised manuscript; J.L. conception and design of research.

## REFERENCES

- Abel ED, Kaulbach HC, Tian R, Hopkins JC, Duffy J, Doetschman T, Minnemann T, Boers ME, Hadro E, Oberste-Berghaus C, Quist W, Lowell BB, Ingwall JS, Kahn BB. Cardiac hypertrophy with preserved contractile function after selective deletion of GLUT4 from the heart. *J Clin Invest* 104: 1703–1714, 1999.
- Albiston AL, Yeatman HR, Pham V, Fuller SJ, Diwakarla S, Fernando RN, Chai SY. Distinct distribution of GLUT4 and insulin regulated aminopeptidase in the mouse kidney. *Regul Pept* 166: 83–89, 2011.
- Alves DS, Farr GA, Seo-Mayer P, Caplan MJ. AS160 associates with the Na<sup>+</sup>/K<sup>+</sup>-ATPase and mediates the adenosine monophosphate-stimulated protein kinase-dependent regulation of sodium pump surface expression. *Mol Biol Cell* 21: 4400–4408, 2010.
- Alves DS, Thulin G, Loffing J, Kashgarian M, Caplan MJ. Akt Substrate of 160 kD regulates Na<sup>+</sup>/K<sup>+</sup>-ATPase trafficking in response to energy depletion and renal ischemia. *J Am Soc Nephrol* pii: ASN.2013101040, 2015.
- Anderson TJ, Martin S, Berka JL, James DE, Slot JW, Stow JL. Distinct localization of renin and GLUT-4 in juxtaglomerular cells of mouse kidney. *Am J Physiol Renal Physiol* 274: F26–F33, 1998.
- Bagnasco S, Good D, Balaban R, Burg M. Lactate production in isolated segments of the rat nephron. *Am J Physiol Renal Fluid Electrolyte Physiol* 248: F522–F526, 1985.
- Barr F, Lambright DG. Rab GEFs and GAPs. *Curr Opin Cell Biol* 22: 461–470, 2010.
- Bouzakri K, Ribaux P, Tomas A, Parnaud G, Rickenbach K, Halban PA. Rab GTPase-activating protein AS160 is a major downstream effector of protein kinase B/Akt signaling in pancreatic beta-cells. *Diabetes* 57: 1195–1204, 2008.
- Brosius FC, Briggs JP, Marcus RG, Barac-Nieto M, Charron MJ. Insulin-responsive glucose transporter expression in renal microvessels and glomeruli. *Kidney Int* 42: 1086–1092, 1992.
- Cao S, Li B, Yi X, Chang B, Zhu B, Lian Z, Zhang Z, Zhao G, Liu H, Zhang H. Effects of exercise on AMPK signaling and downstream components to PI3K in rat with type 2 diabetes. *PLoS One* 7: e51709, 2012.
- Cartee GD, Funai K. Exercise and insulin: Convergence or divergence at AS160 and TBC1D1? *Exerc Sport Sci Rev* 37: 188–195, 2009.
- Chabardès-Garonne D, Mejean A, Aude JC, Cheval L, Di Stefano A, Gaillard MC, Imbert-Teboul M, Wittner M, Balian C, Anthouard V, Robert C, Séguens B, Wincker P, Weissenbach J, Doucet A, Elalouf JM. A panoramic view of gene expression in the human kidney. *Proc Natl Acad Sci USA* 100: 13710–13715, 2003.
- Chadt A, Immisch A, De Wendt C, Springer C, Zhou Z, Stermann T, Holman GD, Loffing-Cueni D, Loffing J, Joost HG, Al-Hasani H. Deletion of both Rab-GTPase-activating proteins TBC14KO and TBC1D4 in mice eliminates insulin- and AICAR-stimulated glucose transport. *Diabetes* 64: 746–759, 2015.
- Chadt A, Leicht K, Deshmukh A, Jiang LQ, Scherneck S, Bernhardt U, Dreja T, Vogel H, Schmolz K, Kluge R, Zierath JR, Hultschig C, Hoeben RC, Schürmann A, Joost HG, Al-Hasani H. Tbc1d1 mutation in lean mouse strain confers leanness and protects from diet-induced obesity. *Nat Genet* 40: 1354–1359, 2008.
- Chin E, Zhou J, Bondy C. Anatomical and developmental patterns of facilitative glucose transporter gene expression in the rat kidney. *J Clin Invest* 91: 1810–1815, 1993.
- Comellas AP, Kelly AM, Trejo HE, Briva A, Lee J, Sznajder JJ, Dada LA. Insulin regulates alveolar epithelial function by inducing Na<sup>+</sup>/K<sup>+</sup>-ATPase translocation to the plasma membrane in a process mediated by the action of Akt. *J Cell Sci* 123: 1343–1351, 2010.
- Dash S, Sano H, Rochford JJ, Semple RK, Yeo G, Hyden CSS, Soos MA, Clark J, Rodin A, Langenberg C, Druet C, Fawcett KA, Tung YCL, Wareham NJ, Barroso I, Lienhard GE, O'Rahilly S, Savage DB. A truncation mutation in TBC1D4 in a family with acanthosis nigricans and postprandial hyperinsulinemia. *Proc Natl Acad Sci USA* 106: 9350–9355, 2009.
- Eguez L, Lee A, Chavez JA, Miinea CP, Kane S, Lienhard GE, McGraw TE. Full intracellular retention of GLUT4 requires AS160 Rab GTPase activating protein. *Cell Metab* 2: 263–272, 2005.
- Faresse N, Lagnaz D, Debonneville A, Ismailji A, Maillard M, Fejes-Toth G, Náráy-Fejes-Tóth A, Staub O. Inducible kidney-specific Sgk1 knockout mice show a salt-losing phenotype. *Am J Physiol Renal Physiol* 302: F977–F985, 2012.
- Férelle E, Carranza ML, Gonin S, Béguin P, Pedemonte C, Rousselot M, Caverzasio J, Geering K, Martin PY, Favre H. Insulin-induced stimulation of Na(+),K(+)-ATPase activity in kidney proximal tubule cells depends on phosphorylation of the alpha-subunit at Tyr-10. *Mol Biol Cell* 10: 2847–2859, 1999.
- Frasa MAM, Koessmeier KT, Ahmadian MR, Braga VMM. Illuminating the functional and structural repertoire of human TBC/RABGAPs. *Nat Rev Mol Cell Biol* 13: 67–73, 2012.
- Glaudemans B, Terryn S, Götz N, Brunati M, Cattaneo A, Bachi A, Al-Qusairi L, Ziegler U, Staub O, Rampoldi L, Devuyst O. A primary culture system of mouse thick ascending limb cells with preserved function and uromodulin processing. *Pflügers Arch* 466: 343–356, 2014.
- Guder WG, Ross BD. Enzyme distribution along the nephron. *Kidney Int* 26: 101–111, 1984.
- Gunaratne R, Braucht DWW, Rinschen MM, Chou CL, Hoffert JD, Pisitkun T, Knepper MA. Quantitative phosphoproteomic analysis reveals cAMP/vasopressin-dependent signaling pathways in native renal thick ascending limb cells. *Proc Natl Acad Sci USA* 107: 15653–15658, 2010.
- Hall AM, Unwin RJ, Parker N, Duchon MR. Multiphoton imaging reveals differences in mitochondrial function between nephron segments. *J Am Soc Nephrol Nephrol* 20: 1293–1302, 2009.
- Hresko RC, Hruz PW. HIV protease inhibitors act as competitive inhibitors of the cytoplasmic glucose binding site of GLUTs with differing affinities for GLUT1 and GLUT4. *PLoS One* 6: e25237, 2011.
- Jung HJ, Kwon TH. Membrane trafficking of collecting duct water channel protein AQP2 regulated by Akt/AS160. *Electrolyte Blood Press* 8: 59–65, 2010.
- Kane S, Sano H, Liu SCH, Asara JM, Lane WS, Garner CC, Lienhard GE. A method to identify serine kinase substrates. Akt phosphorylates a novel adipocyte protein with a Rab GTPase-activating protein (GAP) domain. *J Biol Chem* 277: 22115–22118, 2002.
- Kim HY, Choi HJ, Lim JS, Park EJ, Jung HJ, Lee YJ, Kim SY, Kwon TH. Emerging role of Akt substrate protein AS160 in the regulation of AQP2 translocation. *Am J Physiol Renal Physiol* 301: F151–F161, 2011.
- Kortenoeven MLA, Pedersen NB, Miller RL, Rojek A, Fenton RA. Genetic ablation of aquaporin-2 in the mouse connecting tubules results in defective renal water handling. *J Physiol* 591: 2205–2219, 2013.
- Lansey MN, Walker NN, Hargett SR, Stevens JR, Keller SR. Deletion of Rab GAP AS160 modifies glucose uptake and GLUT4 translocation in primary skeletal muscles and adipocytes and impairs glucose homeostasis. *Am J Physiol Endocrinol Metab* 303: E1273–E1286, 2012.
- Lee JW, Chou CL, Knepper AM. Deep Sequencing in Microdissected Renal Tubules Identifies Nephron Segment-Specific Transcriptomes. *J Am Soc Nephrol* pii: ASN.2014111067, 2015.
- Leto D, Saltiel AR. Regulation of glucose transport by insulin: traffic control of GLUT4. *Nat Rev Mol Cell Biol* 13: 383–396, 2012.
- Liang X, Butterworth MB, Peters KW, Frizzell RA. AS160 modulates aldosterone-stimulated epithelial sodium channel forward trafficking. *Mol Biol Cell* 21: 2024–2033, 2010.
- Lier N, Gresko N, Di Chiara M, Loffing-Cueni D, Loffing J. Immunofluorescent localization of the Rab-GAP protein TBC1D4 (AS160) in mouse kidney. *Histochem Cell* 138: 101–112, 2012.
- Loffing J, Korbacher C. Regulated sodium transport in the renal connecting tubule (CNT) via the epithelial sodium channel (ENaC). *Pflügers Arch* 458: 111–135, 2009.
- Loffing J, Loffing-Cueni D, Valderrabano V, Kläusli L, Hebert SC, Rossier BC, Hoenderop JG, Bindels RJ, Kaissling B. Distribution of transcellular calcium and sodium transport pathways along mouse distal nephron. *Am J Physiol Renal Physiol* 281: F1021–F1027, 2001.
- Meyer AH, Katona I, Blatow M, Rozov A, Monyer H. In vivo labeling of parvalbumin-positive interneurons and analysis of electrical coupling in identified neurons. *J Neurosci* 22: 7055–7064, 2002.
- Moeller HB, Fenton RA. Cell biology of vasopressin-regulated aquaporin-2 trafficking. *Pflügers Arch* 464: 133–144, 2012.



40. Moltke I, Grarup N, Jørgensen ME, Bjerregaard P, Treebak JT, Fumagalli M, Korneliussen TS, Andersen MA, Nielsen TS, Krarup NT, Gjesing AP, Zierath JR, Linneberg A, Wu X, Sun G, Jin X, Al-Aama J, Wang J, Borch-Johnsen K, Pedersen O, Nielsen R, Albrechtsen A, Hansen T. A common Greenlandic TBC1D4 variant confers muscle insulin resistance and type 2 diabetes. *Nature* 512: 190–193, 2014.
41. Picard N, Trompf K, Yang CL, Miller RL, Carrel M, Loffing-Cueni D, Fenton RA, Ellison DH, Loffing J. Protein phosphatase 1 inhibitor-1 deficiency reduces phosphorylation of renal NaCl cotransporter and causes arterial hypotension. *J Am Soc Nephrol* 25: 511–522, 2014.
42. Pradervand S, Wang Q, Burnier M, Beermann F, Horisberger JD, Hummler E, Rossier BC. A mouse model for Liddle's syndrome. *J Am Soc Nephrol* 10: 2527–2533, 1999.
43. Pradervand S, Zuber Mercier A, Centeno G, Bonny O, Firsov D. A comprehensive analysis of gene expression profiles in distal parts of the mouse renal tubule. *Pflügers Arch* 460: 925–952, 2010.
44. Reilly RF, Ellison DH. Mammalian distal tubule: physiology, pathophysiology, and molecular anatomy. *Physiol Rev* 80: 277–313, 2000.
45. Rojek A, Füchtbauer EM, Kwon TH, Frøkiaer J, Nielsen S. Severe urinary concentrating defect in renal collecting duct-selective AQP2 conditional-knockout mice. *Proc Natl Acad Sci USA* 103: 6037–6042, 2006.
46. Ronzaud C, Loffing-Cueni D, Hausel P, Debonneville A, Malsure SR, Fowler-Jaeger N, Boase NA, Perrier R, Maillard M, Yang B, Stokes JB, Koesters R, Kumar S, Hummler E, Loffing J, Staub O. Renal tubular NEDD4-2 deficiency causes NCC-mediated salt-dependent hypertension. *J Clin Invest* 123: 657–665, 2013.
47. Ross BD, Espinal J, Silva P. Glucose metabolism in renal tubular function. *Kidney Int* 29: 54–67, 1986.
48. Sakamoto K, Holman GD. Emerging role for AS160/TBC1D4 and TBC1D1 in the regulation of GLUT4 traffic. *Am J Physiol Endocrinol Metab* 295: E29–E37, 2008.
49. Sano H, Eguez L, Teruel MN, Fukuda M, Chuang TD, Chavez JA, Lienhard GE, McGraw TE. Rab10, a target of the AS160 Rab GAP, is required for insulin-stimulated translocation of GLUT4 to the adipocyte plasma membrane. *Cell Metab* 5: 293–303, 2007.
50. Sano H, Kane S, Sano E, Miinea CP, Asara JM, Lane WS, Garner CW, Lienhard GE. Insulin-stimulated phosphorylation of a Rab GTPase-activating protein regulates GLUT4 translocation. *J Biol Chem* 278: 14599–14602, 2003.
51. Shimkets RA, Warnock DG, Bositis CM, Nelson-Williams C, Hansson JH, Schambelan M, Gill JR, Ulick S, Milora RV, Findling JW. Liddle's syndrome: heritable human hypertension caused by mutations in the beta subunit of the epithelial sodium channel. *Cell* 79: 407–414, 1994.
52. Sorensen MV, Grossmann S, Roesinger M, Gresko N, Todkar AP, Barmettler G, Ziegler U, Odermatt A, Loffing-Cueni D, Loffing J. Rapid dephosphorylation of the renal sodium chloride cotransporter in response to oral potassium intake in mice. *Kidney Int* 83: 811–824, 2013.
53. Stenmark H, Olkkonen VM. The Rab GTPase family. *Genome Biol* 2: REVIEWS3007, 2001.
54. Todkar A, Di Chiara M, Loffing-Cueni D, Bettoni C, Mohaupt M, Loffing J, Wagner CA. Aldosterone deficiency adversely affects pregnancy outcome in mice. *Pflügers Arch* 464: 331–343, 2012.
55. Treebak JT, Taylor EB, Witczak CA, An D, Toyoda T, Koh HJ, Xie J, Feener EP, Wojtaszewski JFP, Hirshman MF, Goodyear LJ. Identification of a novel phosphorylation site on TBC1D4 regulated by AMP-activated protein kinase in skeletal muscle. *Am J Physiol Cell Physiol* 298: C377–C385, 2010.
56. Wagner CA, Loffing-Cueni D, Yan Q, Schulz N, Fakitsas P, Carrel M, Wang T, Verrey F, Geibel JP, Giebisch G, Hebert SC, Loffing J. Mouse model of type II Bartter's syndrome. II. Altered expression of renal sodium- and water-transporting proteins. *Am J Physiol Renal Physiol* 294: F1373–F1380, 2008.
57. Wang HY, Ducommun S, Quan C, Xie B, Li M, Wasserman DH, Sakamoto K, Mackintosh C, Chen S. AS160 deficiency causes whole-body insulin resistance via composite effects in multiple tissues. *Biochem J* 449: 479–489, 2013.
58. Zerial M, McBride H. Rab proteins as membrane organizers. *Nature Rev Mol Cell Biol* 2: 107–117, 2001.
59. Zuber AM, Singer D, Penninger JM, Rossier BC, Firsov D. Increased renal responsiveness to vasopressin and enhanced V2 receptor signaling in RGS2<sup>-/-</sup> mice. *J Am Soc Nephrol* 18: 1672–1678, 2007.